Supporting Information

Hyperpolarized [^{15}N]nitrate as a potential long lived hyperpolarized contrast agent for MRI

Ayelet Gamliel, Sivaranjan Uppala, Gal Sapir, Talia Harris, Atara Nardi-Schreiber, David Shaul, Jacob Sosna, J. Moshe Gomori, and Rachel Katz-Brull

S1. T_1 values and enhancement factors of hyperpolarized [^{15}N]nitrate in individual dissolutions

Various parameters in these experiments were modified to support the multiple questions presented in this study, therefore, the enhancement factor data cannot be averaged. The maximal value is reported in the main text (Experiment No. 2 in Table S1). Enhancement factors were calculated with reference to a spectrum of the same sample in the same spectrometer used to record the hyperpolarized signal (5.8T), as described in the Methods section.

Table S1. T_1 values and enhancement factors determined on hyperpolarized [^{15}N]nitrate dissolution experiments

Experiment No.	[NO_3^-] in NMR tube (mM)	Solvent for dissolution	Frequency of irradiation (GHz)	Polarization Time (min)	Temperature range (°C)	$^{15}NO_3^-$ T_1 (s)	Enhancement Factor at 5.8 T	Polarization (%)
1	26.4	H_2O	94.116	157	36.6-39	94	4,281	0.82
2	29.3	H_2O	94.100	150	34.3-40.4	102	5,298	1.02
3	28.3	Saline + 10% D_2O	94.116	150	36.6-41.4	99	3,080	0.59
4	17.9	Saline + Saliva	94.100	128	37-41.8	106	Not determined	-
5	21.9	D_2O	94.116	30	37.2-41.4	100	1,824	0.35
6	21.8	D_2O	94.116	60	37-39.2	109	2,339	0.45
7	21.7	D_2O	94.116	105	36-40.2	118	2,709	0.52
8	27.5	D_2O	94.116	164	36.5-44	122	4,709	0.90
9	27.3	D_2O	94.116	256	38.5-43	**	4,024	0.77
10	21.8	D_2O	94.110	30	38-42	105	2,162	0.41
11	21.6	D_2O	94.122	30	35.5-39	**	1,647	0.32
12	21.1	D_2O	94.092	30	36.4-40.4	**	3,180	0.61
13	18.7	D_2O	94.104	30	36-41.5	98	3,228	0.62
14	22.2	D_2O	94.098	30	39.3-42.5	107	2,965	0.57
15	22.1	D_2O	94.128	30	38.6-41.5	99	1,436	0.28
16	22.2	D_2O	94.134	30	38.8-41	112	756	0.14
17	20.8	D_2O	94.086	30	38.1-39.6	117	3,894	0.75
18	20.1	D_2O	94.146	30	39-42.6	102	1,166	0.22
19	18.8	D_2O	94.080	30	Not recorded	**	3,778	0.72
20	23	D_2O	94.152	30	39.6-49.8	105*	1,615	0.31
21	29	D_2O	94.100	150	37-42	125	Not determined	-

*The T_1 of this experiment is not included in Figure 1b (T_1 determinations) because the temperature was too high. ** The T_1 of these measurements is not reported due to the following reasons: temperature not recorded (19) and insufficient confidence interval (9, 11, 12).

S2. Long term monitoring of the conversion of [^{15}N]nitrate to [^{15}N]nitrite in solutions containing human saliva

The same sample of sodium [^{15}N]nitrate in the saline-saliva solution presented in Figure 2g (which did not show metabolism) was scanned about a month later and showed about equal signals of [^{15}N]nitrate and [^{15}N]nitrite. To investigate the stability of the [^{15}N]nitrate in saline and saline-saliva solutions using controlled conditions, this experiment was repeated in the following way. First we investigated the stability of [^{15}N]nitrate in the saline solution. In order to mimic the experiment with hyperpolarized [^{15}N]nitrate in terms of the DNP formulation and the dissolution components, 9.97 mg of [^{15}N]nitrate and 2.60 mg of glucose were dissolved in 26.15 mg of a D_2O:glycerol mixture (66:34). Then, 4.59 mL saline and 0.66 mL of D_2O were added to this mixture. This solution was transferred to an NMR tube and scanned for 5 days. ^{15}N fully-relaxed spectra were recorded in blocks of about 4 h, whereas each block consisted of 720 averages with a 30° flip angle and a repetition time of 20 s. The summation of this 5 days scan is shown in Figure S2a. Only the [^{15}N]nitrate signal appears in the spectrum, suggesting that [^{15}N]nitrate is stable at room temperature in this solution for this period time.

In the next step, this solution was divided into 2 samples, in the following manner: 3 mL of this solution were combined with 0.75 mL of human saliva and the combined solution was scanned for 5 days. The rest of the solution (without human saliva) was kept outside the magnet at room temperature. The resulting spectrum of the [^{15}N]nitrate in the saline-saliva solution (Figure S2b) shows the signal of [^{15}N]nitrite in addition to [^{15}N]nitrate, suggesting conversion due to the bacteria in the saliva. Figure S2c shows the resulting spectrum of an additional 5 days scan of the [^{15}N]nitrate in saline solution without human saliva. Despite the longer duration of presence of [^{15}N]nitrate in saline, exposed to environmental bacteria, no conversion to [^{15}N]nitrite was observed. These results suggest that [^{15}N]nitrate in saline solution is stable at room temperature for at least 19 days (10 days of actual measurements and 9 days in between measurements). In addition, it suggests that the conversion to [^{15}N]nitrite was indeed catalyzed by human saliva microbiome. The conversion rate appeared to be about 23% in 5 days in a solution with a starting [^{15}N]nitrate concentration of 22 mM. Assuming a linear conversion rate of nitrate to nitrite, the conversion rate appears to be about 3.8 µmole per day per 0.75 mL of saliva. The entire study was carried out using non-sterile lab ware to allow environmental bacteria to show effect – if any.

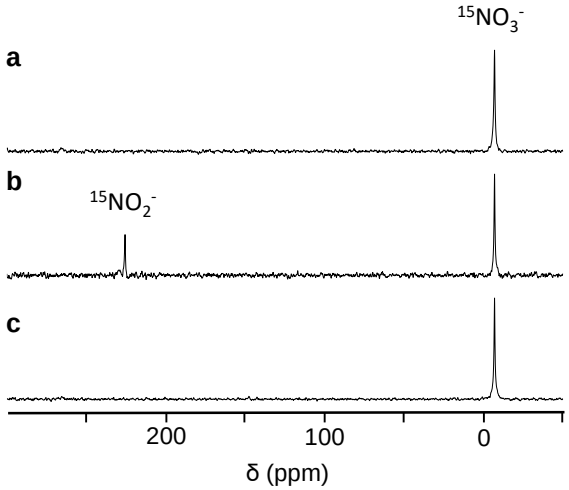

Figure S2. ^{15}N-NMR long term monitoring of [^{15}N]nitrate metabolism in saline and in saline-saliva solution.

a) A solution containing sodium [^{15}N]nitrate (22 mM) and glucose (2.7 mM) in saline, scanned for 5 days. b) A solution containing 3mL of the solution in (a) combined with 0.75 mL of human saliva, scanned for 5 days. The ratio of the [^{15}N]nitrite to [^{15}N]nitrate integrals is about 3:10. c) The same solution as in (a), scanned for 5 days. The scan started after 14 days at room temperature.

S3. Determination of the solid-state build-up time constant

In order to find the optimal polarization time, a series of 5 dissolution experiments was performed in which the time for solid-state polarization buildup by the DNP process was varied from 30 min to 256 min. The microwave frequency was 94.116 GHz and the microwave power was 100mW. Each point was calculated by dividing the enhancement factor of the hyperpolarized [^{15}N]nitrate signal in the solution by the [^{15}N]nitrate concentration in the solution.

Determination of the solid-state build-up time constant was performed by curve fitting of the data to the following equation: $P(t) = P_{max} * \left(1 - e^{\left(\frac{-t}{BU}\right)}\right)$ where BU is the build-up time constant. The build-up time constant was about 75 min. This result suggested that about 4 h of polarization are required to reach 96% of the maximal polarization level for this sodium [^{15}N]nitrate formulation.

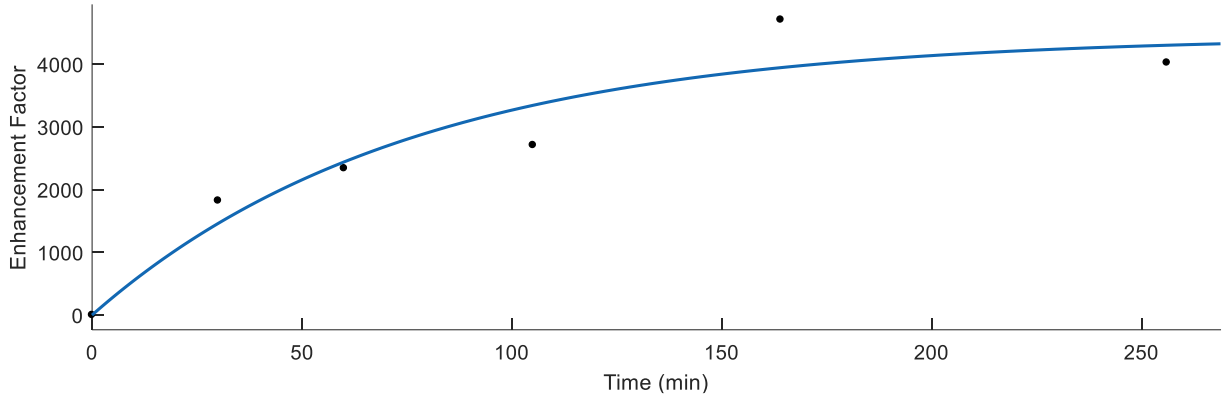

Figure S3. The dependence of the enhancement factors of the [^{15}N]nitrate hyperpolarized signal in solution on the polarization time in solid-state.

S4. Optimization of microwave frequency for irradiation

To select the microwave frequency for the current study, a series of dissolution experiments was performed in which only the microwave frequency for solid-state polarization buildup by the DNP process was varied. Initially we worked according to the previously recommended microwave frequency by Raynolds *et al.* [47], who found that the microwave irradiation frequency required for DNP of the ^{15}N nuclei was similar to that of ^{13}C nuclei in a pyruvate formulation. The results

shown in Figure S5 demonstrate that a slightly different frequency may be more adequate in the particular formulations used in our lab.

Each point of ^{15}N polarization in Figure S5 is the result of a polarization at the indicated microwave frequency for 0.5 h with a microwave power of 100 mW. Dissolution was performed in 4 mL of D_2O. The ^{15}N spectra were recorded with a 30° flip angle and a repetition time of 2 s. The highest signal in each decay series was used for the calculation of relative polarization level. After a series of a few such high flip angle pulses, the rest of the decay was sampled with 10° pulses and longer repetition times (up to 8 s) and this part of the data was used for T_1 calculations as shown in Figures 1 and 3 in the text.

Sources of variability in such a measurement consist of inconsistent duration from the dissolution to recording of the specific spectrum used for evaluation and non-homogeneous dissolution- *i.e.* the possibility that only part of the material placed in the polarization cup is visible to the solution-state spectrometer probe, variation in magnetic field homogeneity, and variation in probe tuning and/or pulse calibration. Despite all of these sources of variability, an optimal frequency for irradiation appears to be at 94.100 GHz and this frequency was used throughout the current study (unless otherwise stated).

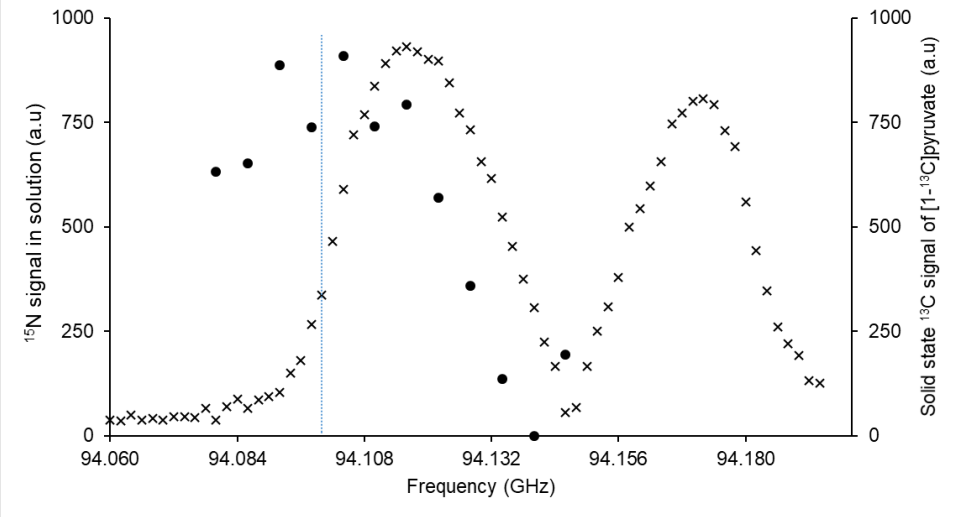

Figure S4. The dependence of the [^{15}N]nitrate hyperpolarized signal amplitude in solution on the solid-state microwave irradiation frequency.

The solid-state polarization build-up of [1-^{13}C]pyruvic acid (×) was determined in solid-state using a 5° flip angle and a buildup time of 0.5 min for each point. The microwave power was 100 mW. The pyruvic acid formulation contained 94.93 mg of neat [1-^{13}C]pyruvic acid and 1.70 mg of

OXO63 radical. 25.82 mg of this formulation were used. The polarization buildup is presented in arbitrary units obtained from the polarizer interface. For the purpose of presentation on the same graph with the nitrate polarization these arbitrary values were divided by the weight of the sample (the same sample used for all data points) and by the duration of the polarization, and then multiplied by 3000 (Y-axis on the right).
The solid-state polarization build-up of sodium [^{15}N]nitrate (●) was determined in the dissolved samples, *i.e.* in solution. The SNR of the sodium [^{15}N]nitrate signal in solution in ^{15}N magnitude spectra, was multiplied by the linewidth at half-height and divided by the nitrate formulation weight. The blue dotted line indicates the microwave frequency selected for irradiation of the sodium [^{15}N]nitrate in the current study (0.012 GHz less than the optimal frequency of irradiation for pyruvic acid).

S5. Monitoring of sample temperature during the NMR measurements and simultaneous T_1 determinations

The temperature of the solutions in the NMR tubes was monitored during the NMR measurements with an MRI compatible temperature sensor. Two examples of such simultaneous temperature monitoring and hyperpolarized ^{15}N-MRS recordings are shown below:

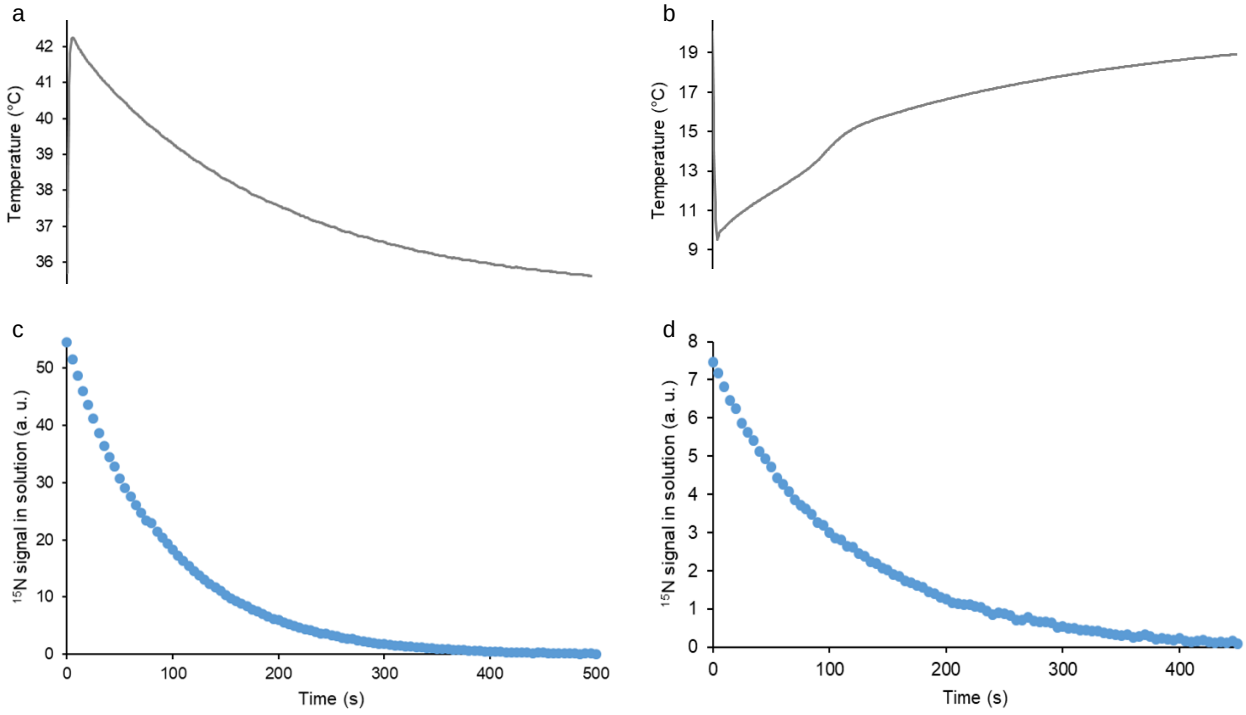

Figure S5. Monitoring of sample temperature in the spectrometer, simultaneously with recordings of the polarization decays.
a) and b) Online temperature recording of hyperpolarized [^{15}N]nitrate solutions within the NMR tube, in the spectrometer. In a), the spectrometer temperature was set to 36 °C and the heating type

was set to 40 °C. The sample arrives to the NMR tube at about 42 °C and cools down to 36 °C during the spectral recording.
b) The spectrometer and the heating tape temperature controllers were turned off, and the 4 mL dissolution medium was cooled by mixing with 4 mL D_2O at 2 °C, the cold medium was injected to the NMR tube within the spectrometer 3 min after the mixing (for additional cooling in the ice-cold water bath). The sample arrived to the NMR spectrometer at about 10 °C and has slowly heated to about 19 °C (approaching room temperature).
c) and d) The hyperpolarized signal decay of the sodium [^{15}N]nitrate in the respective solutions, each point represents the maximal intensity of the signal.
Such measurements enabled the determination of the dependence of the T_1 on the sample temperature.

References

1. M. F. Tweedle, P. Wedeking and K. Kumar, 1995, **30**, 372-380.
2. G. W. White, W. A. Gibby and M. F. Tweedle, 2006, **41**, 272-278.
3. T. Kanda, M. Osawa, H. Oba, K. Toyoda, J. Kotoku, T. Haruyama, K. Takeshita and S. Furui, 2015, **275**, 803-809.
4. Y. Errante, V. Cirimele, C. A. Mallio, V. Di Lazzaro, B. B. Zobel and C. C. Quattrocchi, 2014, **49**, 685-690.
5. E. Kanal and M. F. Tweedle, 2015, **275**, 630-634.
6. T. Kanda, K. Ishii, H. Kawaguchi, K. Kitajima and D. Takenaka, 2014, **270**, 834-841.
7. EMA, EMA's final opinion confirms restrictions on use of linear gadolinium agents in body scans, http://www.ema.europa.eu/ema/index.jsp;curl=pages/medicines/pips/EMEA-001743-PIP01-14/pages/includes/document/pages/includes/document/pages/includes/document/index.jsp?curl=pages/medicines/human/referrals/Gadolinium-containing_contrast_agents/human_referral_prac_000056.jsp&mid=WC0b01ac05805c516f, (accessed Decmber 2018).
8. M. Birka, K. S. Wentker, E. Lusmoller, B. Arheilger, C. A. Wehe, M. Sperling, R. Stadler and U. Karst, 2015, **87**, 3321-3328.
9. M. F. Tweedle, *Magnetic resonance imaging*, 2016, **34**, 1377-1382.
10. E. Kanal, *Magnetic resonance imaging*, 2016, **34**, 1341-1345.
11. P. Marckmann, L. Skov, K. Rossen, A. Dupont, M. B. Damholt, J. G. Heaf and H. S. Thomsen, 2006, **17**, 2359-2362.
12. H. Ersoy and F. J. Rybicki, 2007, **26**, 1190-1197.
13. J. Lohrke, A. L. Frisk, T. Frenzel, L. Schockel, M. Rosenbruch, G. Jost, D. C. Lenhard, M. A. Sieber, V. Nischwitz, A. Kuppers and H. Pietsch, *Investigative radiology*, 2017, DOI: 10.1097/rli.0000000000000344.
14. V. Gulani, F. Calamante, F. G. Shellock, E. Kanal and S. B. Reeder, *The Lancet. Neurology*, 2017, **16**, 564-570.
15. D. L. Archer, *J. Food Prot.*, 2002, **65**, 872-875.
16. E. Weitzberg, M. Hezel and J. O. Lundberg, *Anesthesiology*, 2010, **113**, 1460-1475.
17. S. Shiva, *Redox Biol.*, 2013, **1**, 40-44.
18. R. M. Pluta, E. H. Oldfield, K. D. Bakhtian, A. R. Fathi, R. K. Smith, H. L. DeVroom, M. Nahavandi, S. Woo, W. D. Figg and R. R. Lonser, *PLoS One*, 2011, **6**, 13.
19. J. O. Lundberg and E. Weitzberg, *Gut*, 2013, **62**, 616-629.

20. A. R. Butler and M. Feelisch, *Circulation*, 2008, **117**, 2151-2159.
21. E. F. Sato, T. Choudhury, T. Nishikawa and M. Inoue, *J. Clin. Biochem. Nutr.*, 2008, **42**, 8-13.
22. A. C. Torregrossa, M. Aranke and N. S. Bryan, *J. Geriatr. Cardiol.*, 2011, **8**, 230-242.
23. E. A. Jansson, L. Huang, R. Malkey, M. Govoni, C. Nihlen, A. Olsson, M. Stensdotter, J. Petersson, L. Holm, E. Weitzberg and J. O. Lundberg, *Nat. Chem. Biol.*, 2008, **4**, 411-417.
24. V. Kapil, A. B. Milsom, M. Okorie, S. Maleki-Toyserkani, F. Akram, F. Rehman, S. Arghandawi, V. Pearl, N. Benjamin, S. Loukogeorgakis, R. MacAllister, A. J. Hobbs, A. J. Webb and A. Ahluwalia, *Hypertension*, 2010, **56**, 274-U174.
25. M. R. Duranski, J. J. M. Greer, A. Dejam, S. Jaganmohan, N. Hogg, W. Langston, R. P. Patel, S. F. Yet, X. D. Wang, C. G. Kevil, M. T. Gladwin and D. J. Lefer, *J. Clin. Invest.*, 2005, **115**, 1232-1240.
26. M. Gilchrist, A. C. Shore and N. Benjamin, *Cardiovasc. Res.*, 2011, **89**, 492-498.
27. G. Ellen, P. L. Schuller, E. Bruijns, P. Froeling and H. Baadenhuijsen, *IARC Sci Publ.*, 1982, 365-378.
28. C. Damacena-Angelis, G. H. Oliveira-Paula, L. C. Pinheiro, E. J. Crevelin, R. L. Portella, L. A. B. Moraes and J. E. Tanus-Santos, *Redox Biol.*, 2017, **12**, 291-299.
29. L. D. Roberts, T. Ashmore, A. O. Kotwica, S. A. Murfitt, B. O. Fernandez, M. Feelisch, A. J. Murray and J. L. Griffin, *Diabetes*, 2015, **64**, 471-484.
30. B. L. Loudon, H. Noordali, N. D. Gollop, M. P. Frenneaux and M. Madhani, *Br. J. Pharmacol.*, 2016, **173**, 1911-1924.
31. J. H. Ardenkjaer-Larsen, B. Fridlund, A. Gram, G. Hansson, L. Hansson, M. H. Lerche, R. Servin, M. Thaning and K. Golman, *Proc. Natl. Acad. Sci. U. S. A.*, 2003, **100**, 10158-10163.
32. N. Chattergoon, F. Martinez-Santiesteban, W. B. Handler, J. H. Ardenkjaer-Larsen and T. J. Scholl, *Contrast Media Mol. Imaging*, 2013, **8**, 57-62.
33. M. Fuetterer, J. Busch, S. M. Peereboom, C. von Deuster, L. Wissmann, M. Lipiski, T. Fleischmann, N. Cesarovic, C. T. Stoeck and S. Kozerke, *J. Cardiov. Magn. Reson.*, 2017, **19**, 12.
34. L. L. Lumata, M. E. Merritt, C. R. Malloy, A. D. Sherry, J. van Tol, L. K. Song and Z. Kovacs, *J. Magn. Reson.*, 2013, **227**, 14-19.
35. K. Kumagai, K. Kawashima, M. Akakabe, M. Tsuda, T. Abe and M. Tsuda, *Tetrahedron*, 2013, **69**, 3896-3900.
36. H. Nonaka, M. Hirano, Y. Imakura, Y. Takakusagi, K. Ichikawa and S. Sando, *Sci. Rep.*, 2017, **7**, 6.
37. E. Chiavazza, A. Viale, M. Karlsson and S. Aime, *Contrast Media Mol. Imaging*, 2013, **8**, 417-421.
38. T. Harris, A. Gamliel, S. Uppala, A. Nardi-Schreiber, J. Sosna, J. M. Gomori and R. Katz-Brull, *ChemPhysChem*, 2018, **19**, 2148– 2152.
39. A. W. Barb, S. K. Hekmatyar, J. N. Glushka and J. H. Prestegard, *J. Magn. Reson.*, 2011, **212**, 304-310.
40. C. Gabellieri, S. Reynolds, A. Lavie, G. S. Payne, M. O. Leach and T. R. Eykyn, *J. Am. Chem. Soc.*, 2008, **130**, 4598-+.
41. T. Saluvere and E. Lippmaa, *Chem. Phys. Lett.*, 1970, **7**, 545-548.
42. A. Nardi-Schreiber, A. Gamliel, T. Harris, G. Sapir, J. Sosna, J. M. Gomori and R. Katz-Brull, *Nat. Commun.*, 2017, **8**, 7.
43. H. Allouche-Arnon, T. Wade, L. F. Waldner, V. N. Miller, J. M. Gomori, R. Katz-Brull and C. A. McKenzie, *Contrast Media Mol. Imaging*, 2013, **8**, 72-82.
44. H. Allouche-Arnon, M. H. Lerche, M. Karlsson, R. E. Lenkinski and R. Katz-Brull, 2011, **6**, 499.
45. J. M. Gomori, R. I. Grossman, C. Yu-Ip and T. Asakura, *J. Comput. Assist. Tomogr.*, 1987, **11**, 684-690.
46. M. Karlsson, P. R. Jensen, J. O. Duus, S. Meier and M. H. Lerche, *Appl. Magn. Reson.*, 2012, **43**, 223-236.

47. S. Reynolds and H. Patel, *Appl. Magn. Reson.*, 2008, **34**, 495-508.
48. R. K. Harris, E. D. Becker, S. M. C. De Menezes, R. Goodfellow and P. Granger, *Pure Appl. Chem.*, 2001, **73**, 1795-1818.
49. A. Geissler, K. Kanamori and B. D. Ross, *Biochem. J.*, 1992, **287**, 813-820.
50. P. R. Srinivasan and R. L. Lichter, *J. Magn. Reson.*, 1977, **28**, 227-234.